Journal of the Ghana Institution of Engineering (2024) 24:3
https//doi.org/10.56049/jghie.v24i3.215

ORIGINAL RESEARCH

Flow regime dynamics in a bubble column reactor

Kelvin Aduse-Poku[1], Keren N. M. Hamond[1,*], Kofi A. Busumbru[1], Kwame Sarkodie[1]

Received: 18th July, 2024 / **Accepted:** 22nd October, 2024
Published online: 5th December, 2024

Abstract

This study investigates fluid dynamics within bubble column reactors. Using an air-water system, flow regimes were generated and assessed using predictive models such as homogenous, Armand, and drift flux models. This study highlights the complexities of two-phase fluid flow, particularly focusing on the dynamic behaviours of fluids and bubbles within the column reactor. The experimental setup consisted of a transparent test section, utilizing advanced image processing techniques to accurately determine gas holdups and their relationship with superficial velocities. The results show that the homogenous model effectively predicts the bubble flow regime but encounters limitations in the slug flow regime due to intricate phase interactions and transitional conditions. However, the Armand and drift flux models showed accuracy in the slug and transitional flow regimes and improved at higher superficial liquid velocities. The study underscores the necessity of integrating several empirical models to enhance predictive capabilities in bubble columns. Thus, addressing experimental uncertainties in flow dynamics would be more optimal when other advanced models are integrated in the prediction of multiphase flow regimes.

Keywords: Bubble Column, Flow Regime, Heterogeneous Flow, Homogeneous Flow, Transition, Gas Holdup

Introduction

The complex flow dynamics of two-phase fluid flow in bubble column reactors pose significant challenges. Researchers have developed several models, such as the dispersed bubble, homogeneous flow, and slug flow models, to understand mass and heat transfer, mixing, and reaction kinetics in bubble column reactors. As a result, bubble column reactors have become an essential tool for chemical engineering research and development (Shu *et al*., 2019; Mudde *et al*., 2009; Kantarci *et al*., 2005; Shah *et al*., 1982). This complex phenomenon that occurs in various flow regimes and their impact on reactor performance is not fully understood, which limits the ability to improve the design and operation of these systems in the industry. Optimising the performance of these reactors is challenging due to the dynamic behaviour of the fluid and bubbles within the systems. While several studies have been conducted on these reactors, further research is needed to gain a comprehensive understanding of the complex flow dynamics to optimize reactor performance (Besagni *et al*., 2016; Firouzi and Hashemabadi, 2009; Cheng *et al*., 2008; Kaichiro and Ishii, 1984; Yamaguchi and Yamazaki, 1982). Bubble columns are characterized by extremely complex interactions between phases. As the gas superficial velocity increases in a bubble column with non-foaming liquids, the flow regime progresses from homogeneous to transition to heterogeneous (Besagni *et al*., 2016) as shown in Figure 1.

The interaction between fluids in a bubble column reactor creates complex flow dynamics that can be difficult to predict in terms of flow regime, operability range, scalability, and mixing hydrodynamics. One major limitation of bubble column reactors is their short gas phase residence times due to the high rise in velocities of gas bubbles, which are similar to the slip velocity. In a homogeneous regime of operation, the slip velocity remains fairly constant while it increases with increasing superficial gas velocity in a heterogeneous regime (Hernandez-Alvarado *et al*., 2018). At high gas velocities, the liquid circulation drives out the gas phase, resulting in lower gas phase residence times and low void fractions, reducing maximum gas-liquid contact. As a result, the gas phase residence time in a heterogeneous operation regime is shorter than in a homogeneous regime (Hernandez-Alvarado *et al*., 2018).

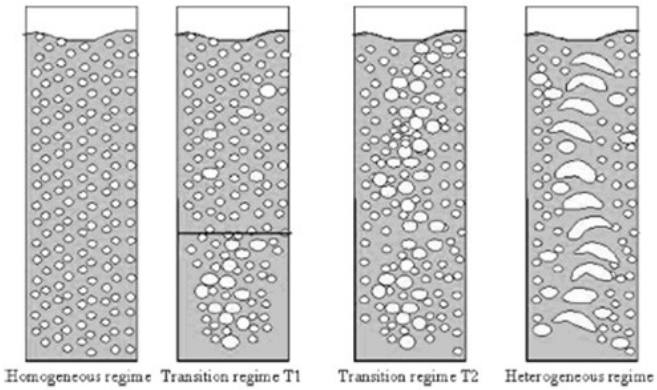

Figure 1 Visual Observations of four flow regimes in bubble columns: Homogeneous, Transition T1, Transition T2, and Heterogeneous (Olmos et al., 2003)

A significant amount of research has been conducted on the transition from homogeneous to heterogeneous flow regimes in bubble column reactors (Zahradnik *et al*., 1997; Shu *et al*., 2019; Mudde *et al.*, 2009). This study focuses on the individual regimes that occur between the homogeneous and transitional regimes. In the homogeneous regime, bubbles are nearly uniform in size and gas holdup is radially uniform. Bubbles rise vertically with minimal transverse and axial oscillations and there is negligible bubble coalescence and breakup in the bed. Bubble size and voidage are determined entirely by gas velocity and the physical properties of the gas-liquid system (Zahradnik *et al*., 1997). Depending on flow rates and gas holdup, a bubble flow regime can be observed in the vertical column flow within the homogeneous region. As the fluid velocity increases, bubbles disperse into more wide spaces, resulting in a dispersed bubbly flow. As gas velocity increases, the heterogeneous regime is observed where bubble interactions become more pronounced. In this regime, the rate of increase in gas holdup is lower than in the homogeneous regime due to the coalescence of smaller bubbles into larger bubbles that ascend at a higher velocity (Zahradnik *et al*., 1997).

Flow regime transition refers to the change in flow patterns within the reactor and can affect the reactor's performance. Different flow regimes can have different gas holdup, mass transfer, and heat transfer characteristics, therefore,

*Corresponding author: kerenhamm@gmail.com

[1]Department of Petroleum Engineering, Faculty of Civil and Geo -Engineering, Kwame Nkrumah University of Science and Technology, Ghana.

understanding and predicting flow regime transitions is important for optimizing the performance of bubble column reactors. (Gong *et al*., 2022). Several models have been proposed to predict different flow regime transitions in bubble column reactors (Besagni *et al*., 2016). These models can provide valuable insights to improve the design and operation of bubble column reactors (BCRs), however, the accuracy and applicability of these models need to be validated with experimental data.

Experimental data can provide a benchmark for assessing the performance of models and can help to identify their strengths and weaknesses (Zahradnik *et al*., 1997). By comparing model predictions with experimental data, researchers can determine how well the models capture the underlying physics of bubble column reactors. This information can be used to improve existing models or to develop new models that better represent the behaviour of fluids in bubble column reactors. Zahradnik *et al*. (1997), Deckwera and Schumpe (1993) and Dhaouadi *et al*. (2008) explored the feasibility of scaling up and designing bubble column reactors for mass transfer applications. They highlighted the complexity of this process due to nonlinear and multidimensional mass transfer phenomena. Scale-up relied on geometric and fluid dynamic similarities, with the gas-liquid mass transfer coefficient being a key parameter. However, the effects of impurities and mixing on mass transfer remained unclear, indicating ongoing research needs. Similarly, Zahradník *et al*. (1997) investigated how gas-liquid flow regimes impacted reactor performance, observing increased gas holdup and mass transfer coefficients during transitions. However, their study was limited to specific conditions and did not consider broader reactor parameters.

Medjiade *et al*. (2017) further explored flow regime transitions, noting increased mass transfer rates during transitions. They emphasized the importance of bubble characteristics in these transitions. However, their study also had limitations in scope and applicability, particularly concerning impurities and industrial-scale relevance. Dhaouadi *et al*. (2008) reviewed gas-liquid mass transfer in bubble columns, identifying key influencing factors such as gas and liquid properties, column geometry, and operating conditions. They emphasized that mass transfer mechanisms are not fully understood, especially in complex systems and non-Newtonian fluids, presenting challenges for scale-up. The review primarily focused on laboratory-scale studies, noting a lack of comprehensive insights for industrial applications.

Lastly, Nguyen *et al*. (2022) utilized computational fluid dynamics to study hydrodynamics in gas-liquid bubble columns under different flow regimes. Their model accurately captured bubble behaviours, with the large eddy simulation approach providing better results despite increased computational time. This study represents a recent advancement in understanding bubble column hydrodynamics.

For this study, Taitel *et al*. (1980) model depicted in Equations (1) and (2) for predicting the flow regime transition from bubble flow to slug regime is used. The transition from bubble to slug flow regime occurs due to the agglomeration and coalescence of bubbles in the bubble flow regime at low liquid flow rates. Taitel *et al*. (1980) showed that vertical co-current upward flow transition takes place when the gas void fraction is greater than 0.25. Substituting this value for the gas void fraction into Equation (2) for the rise velocity of bubbles relative to the average liquid velocity defines the bubble-to-slug transition as:

$$Vs = 3Vsg - 0.75V_{\infty} \quad (1)$$

$$V_{\infty} = 1.58 \sqrt[4]{\frac{g\sigma(\rho_l - \rho_g)}{\rho_l^2}} \quad (2)$$

Where V∞ describes the bubble rise velocity of fairly large bubbles which is quite insensitive to bubble size, Vsg is gas superficial velocity, g is acceleration due gravity, ρ_g is density of gas, ρl is density of liquid and б is surface tension

According to Wu *et al*. (2017) for the bubble-slug transition, the same model used by both Taitel *et al*. (1980) and Armand (1946) given by the two equations (1) and (2) outperformed the work of Mishima and Ishii (1984). Accurate prediction of flow patterns in two-phase systems is essential for the optimal design and operation of various industrial processes. Despite numerous efforts, no universally applicable flow pattern map has been developed, as existing maps are limited by the specific experimental data sets used in their creation. These limitations often lead to discrepancies between studies; for instance, one experiment may report slug flow under specific conditions, while others identify churn or annular flow under similar parameters.

Flow pattern maps are constructed by defining boundaries between different flow regimes, but uncertainty tends to increase near these boundaries. However, further from the transition zones, most maps show consistent alignment. Notable work by Taitel *et al*. (1980) and Mishima and Ishii (1984) have provided equations for the transitions between major flow regimes –such as bubble, slug, churn, and annular flows– based on key parameters like void fraction and fluid velocity. Figure 2 is adapted from the flow pattern map created by Wu *et al*. (2017), which has been validated with a dataset of 2,500 points, demonstrating the boundaries between the observed flow regimes and their transitions.

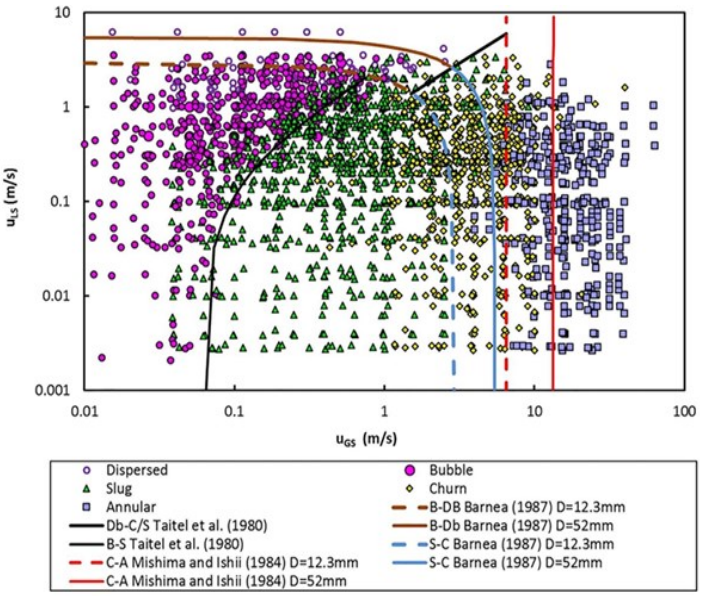

Figure 2 Flow pattern map for vertical upward flow proposed by Wu et al. (2017) where B represents Bubble, D stands for Dispersed, S denotes Slug, C indicates Churn, and A refers to Annular flow

Methodology

Figure 3 shows a schematic diagram of the experimental rig, designed to produce a vertical upward flow of air and water. The rig consists of a 2m transparent test section (TTS) with a 3 -inch external diameter. From Figure 3, the air was delivered by a compressor (COMP), while the water was circulated from a 12L water reservoir using a variable speed water pump (VSWP). Valves (V1 & V2) were used to regulate the water from the reservoir to the TTS. A water flow meter (WFM) was used to measure the water flow rate. The water moves through the water inlet (WI) into the air-water mixer (AWM) after which the air is compressed using a compressor, and the air flow meter (AFM) is used to measure the flow rate through the air inlet (A1).

Water and air were injected into the bottom of the TTS via an air-water mixer, with air injected via a 4 mm pipe fitted with a non-return valve (NRV) at the bottom of the TTS. After the two-phase fluid has circulated through the TTS, it then passes through the horizontal section of diameter 0.5 inches to the vertical return line of diameter 0.5 inches in flexible hose where water is returned to the water reservoir for recirculation. Figure 4 illustrates the laboratory setup, highlighting the key components used in the experiment, including the transparent test section, air-water mixer, and essential instrumentation. The setup in the lab mirrors the schematic presented in Figure 3, providing a real-world view of the experimental apparatus

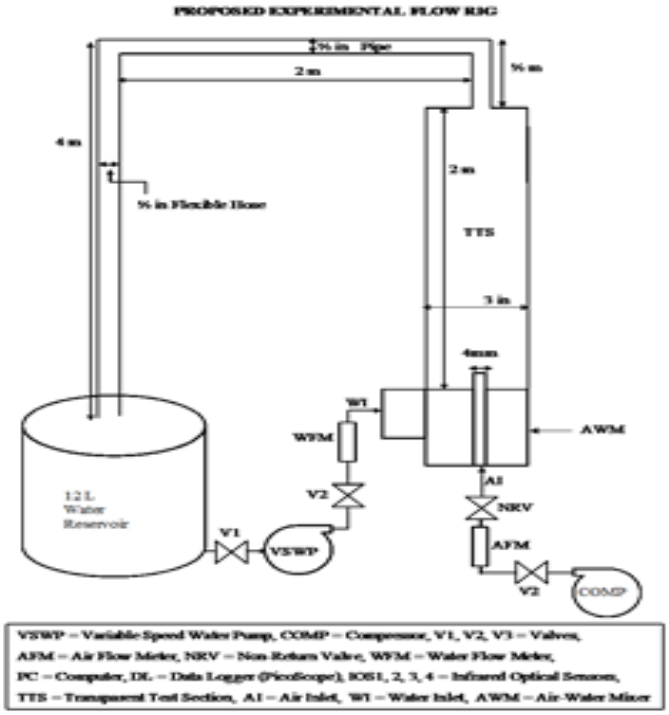

Figure 3 Schematic of the air-water flow rig

A video camera with frame rates of up to 240 frames per second was set up at a distance away to record video focused at a specific control area. A video camera, equipped with an advanced 12-megapixel CMOS (Complementary Metal-Oxide-Semiconductor) sensor, was used to record the experiment. It is important to note that the properties of water and air were obtained from literature at ambient conditions. During the experiment, care was taken to ensure that the viscosity of the water stored in the column reactor and reservoir was not affected by the accumulation of debris. This was done through the regular circulation of water and periodic replenishment of the volumes of water required for the experiments. The outer diameter of the test section is 3 inches while the inner diameter is 2.56 inches. Table 1 presents the flow conditions used during the experiment, including the fluid type, density, viscosity, surface tension, flow rate, and superficial velocity for both air and water. These parameters were carefully controlled to ensure consistent experimental conditions.

Figure 5 illustrates the experimental matrices used during the experiment, showing the relationships between the key variables. These matrices guided the experimental conditions

Figure 4 Two-phase flow experimental setup with 3mm test section with key components labelled 1–9; Note: 1=water reservoir, 2=0.5 in pipe, 3=bubble column, 4=air-water mixer, 5=valves, 6=water pump, 7=air compressor, 8=air flow meter, and 9=water flow meter

under varying flow rates and velocities, which are central to understanding the flow dynamics in the bubble column reactor.

The experimental method

Figure 6 provides a flowchart outlining the experimental procedure followed in the study. This visual representation details each step from the initial setup of the bubble column reactor to the final analysis of gas holdups using image processing techniques. The flowchart serves as a guide to the methodology employed in the experiments. Due to the length of the bubble column, the whole section of the bubble column

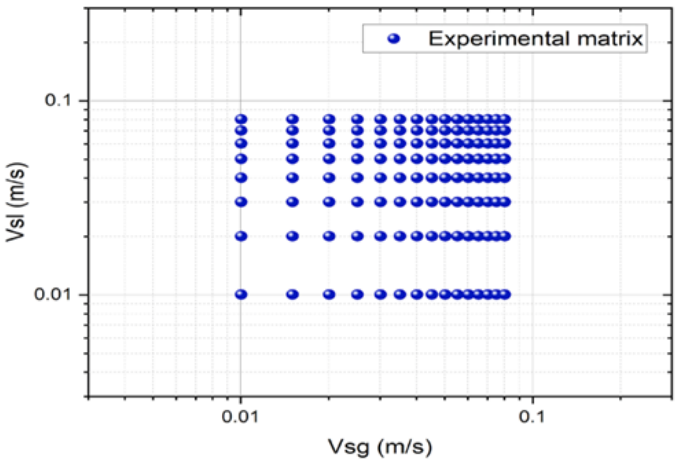

Figure 5 Experimental matrices depicting flow conditions for superficial gas and liquid velocities

Table 1 Summary of fluid conditions

Fluid Type	Density (kg/m^3)	Viscosity (cp)	Surface tension (N/m)	Flow rate (m^3/s)	Superficial velocity (m/s)
Water	997.0	0.890	0.0728	0-0.000267	0-0.0803
Air	1.184	0.018	Negligible	0-0.000267	0-0.0803

cannot be taken into consideration. The video camera was focused on the specific control area after the field of view was set, and video footage was taken for each experimental matrix. The system was allowed to be steady for some time before different videos were recorded. These recorded footages require extensive processing to estimate void fractions and determine flow regimes of the flow.

The photo frames from the footage are converted to distinct images for each flow condition using the Windows Photo application on a computer. Photo frames were acquired in Red-Green-Blue (RGB) format. It is essential to adhere to image format and resolution requirements for all the different matrices to improve accuracy during image analysis. Consistency in lighting conditions and a well-controlled background were crucial in minimizing noise and ensuring reliable results.

Acquired images were processed with the use of ImageJ software. Before phase fraction determination, pre-processing steps were applied to enhance the quality of the images. Image calibration and scaling were performed to ensure accurate measurements. Various noise reduction techniques were employed to reduce unwanted noise and enhance the signal-to-noise ratio. Image threshold techniques were used to separate the air and water phases, facilitating subsequent analysis.

The images were converted from RGB to grayscale. The grayscale image was processed using a Fast Fourier Transform (FFT) bandpass filter selected to optimize the visibility of the entrained bubbles by suppressing the liquid slug background. The enhanced grayscale image was then converted to a binary scale image. Figure 7 illustrates the stages of image processing applied to the frames captured during the experiment. This includes the transformation from the original Red-Green-Blue (RGB) images (Figure 7a) to grayscale (Figure 7b), saturated (Figure 7c), and binary scale images (Figure 7d). These stages are crucial for improving the visibility of bubbles and accurately calculating gas holdup during the analysis. Based on the experimental data, the processed images serve as the foundation for determining void fractions and flow regimes. By analysing images obtained during experiments, this methodology quantitatively assesses the proportions of air and water phases present during each condition of the specific superficial velocity.

The gas holdup is a dimensionless key parameter for design purposes that is defined here as the area occupied by the gas bubbles within the field of view. Areal void fractions were determined from the total area occupied by air bubbles in the control section using the imaging processing technique. Using the ImageJ application, the region of interest or area of entrained bubbles was selected considering the air-water interface. Through image segmentation using the threshold images, the individual regions corresponding to air and water phases were identified. The area, or pixel count of each segmented region was measured to determine the respective phase fractions. These void fractions were calculated as a ratio of the segmented area to the total area of the control section as:

$$\mathcal{E} = \frac{Ag}{A_\tau} \qquad (3)$$

where ε is the gas holdup, A_g is the area covered by air, and A_T is the area covered by the control section.

Void fractions obtained via the image processing techniques were validated with already-developed models to ensure their accuracy and reliability. Calibration was performed by comparing the results obtained through image processing with reference measurements or analytical techniques. This helps to establish the robustness of the technique in determining phase fractions of the air-water system in the 3-in-diameter bubble column reactor. Three developed models, viz homogenous, Armand and drift flux models, were used in the gas holdup validation.

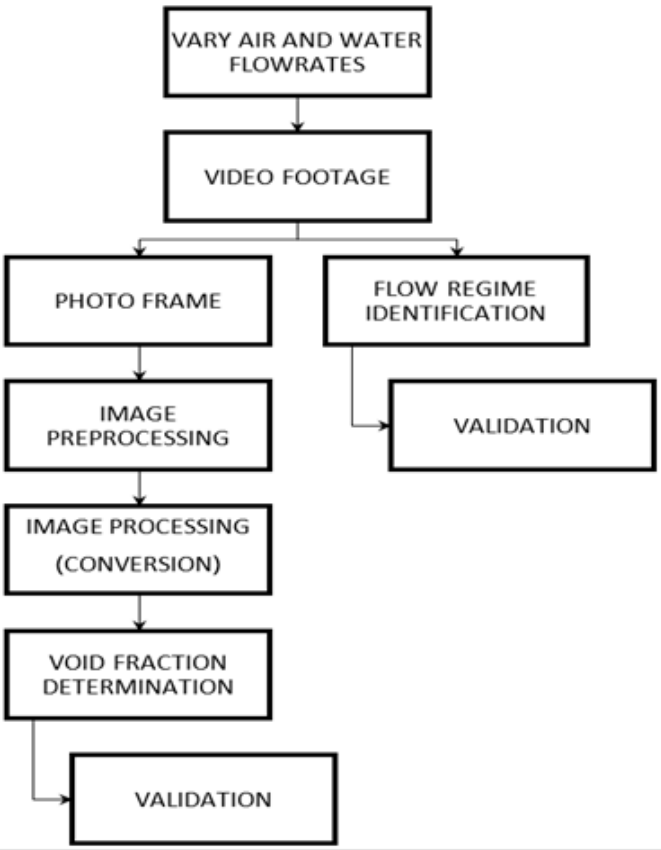

Figure 6 Flowchart showing the experimental procedure for two -phase flow testing

Homogenous model

The homogeneous model assumes that the gas and liquid phases within the bubble column are perfectly mixed and uniformly distributed. The homogenous model computes the void fraction based on no-slip assumptions between each flowing phase. This model simplifies the complex interactions between bubbles and liquid and is based on mass and momentum balance equations. While it is a simple approach, it might not capture the actual behaviour of the column accurately, especially in situations where phase separation and bubble coalescence play a significant role. The model is given as:

$$\varepsilon_H = \frac{V_{sg}}{V_{sl} + V_{sg}} \qquad (4)$$

Where ε_H is the void fraction by the Homogenous model, Vsg is the superficial gas velocity, and Vsl is the superficial liquid velocity.

Armand (1946) model

The Armand (1946) model improves upon the homogeneous model by considering the effects of slip conditions between the air and water. It considers different bubble sizes and their rise velocities, which influence the void fraction. The model considers a constant multiple or some function against the no-slip (homogeneous) void fraction correlation, ε_H. To predict the void fraction taking into consideration the non-homogeneous nature of the two-phase flow, Armand (1946) and Nicklin (1962) gave the correlation:

$$\varepsilon A = K \times \varepsilon H \qquad (5)$$

Where εA is the void fraction by Armand (1946) model (Nicklin, 1962), εH is the void fraction by the Homogenous model, and K is a constant multiple; for Armand (1946) correlation, the K value is 0.833.

Drift Flux Model

The drift-flux (Zuber and Findlay, 1965) is defined as the relative motion of a less dense phase (gas) to that of the mixture of the two phases (gas and liquid). This drift velocity is related to the slip between gas and liquid velocities respectively as:

$$Vdg = Vg - V_m \text{ and } V_{dl} = V_l - V_m \quad (6)$$

The correlation is more sophisticated and considers the two-phase flow as a combination of a continuous liquid phase and dispersed gas bubbles. It factors in the interactions between bubbles, the liquid phase, and the effects of bubble coalescence and breakup. The model accounts for the relative velocity between the phases, known as the drift velocity, which significantly impacts the void fraction distribution. It is generally considered more accurate than the previous two models in predicting complex two-phase flow behaviour:

$$Vg = C_o \, . \, V_m + V_{dg} \quad (7)$$

To derive the void fraction ε, we start by expressing the mixture velocity Vm as the sum of the superficial liquid velocity V_{sl} and the superficial gas velocity V_{sg}. By substituting this relationship onto equation (7) !

$$V_g = \frac{V_{sg}}{\varepsilon} = C_o \cdot (V_{Sl} + V_{Sg}) + V_{dg} \quad (8)$$

From this, the void fraction can be solved for as:

$$\varepsilon = \frac{V_{sg}}{C_o \, . V_m + V_{dg}} \quad (9)$$

Resulting in the generalized Drift Flux model equation given as:

$$V_{dg} = 0.35.gD \quad (10)$$

Where Vg is the actual gas velocity, D is the internal diameter of the bubble column, Co is the distribution coefficient, V_{sg} is the superficial gas velocity, V_{sl} is the superficial liquid velocity, V_m is the mixture velocity, V_{dg} is the drift velocity relating to gas, V_d is the drift velocity, and V_{dl} is the drift velocity relating to liquid. Co = 1.19 for bubble flow, and Co = 1.20 for slug flow (Zubar and Findlay *et al*. ,1965).

Data in the form of videos recorded in the laboratory was imported into Video-To-Photo software on a computer. The five frames used for the void fraction calculation were cleaned using Image J software. Each image initially in the RGB format is cropped to the correct dimension and converted to a grayscale image. Converting an RGB image to grayscale involves combining the colour channels into one using methods like the Huang model, the luminosity method, and others. The luminosity method calculates the intensity of each pixel based on the weighted average of its red, green, and blue values. The formula is as follows:

$$Grayscale\ value = 0.299 \times red + 0.587 \times green + 0.114 \times blue \quad (11)$$

Grayscale-converted images are cleaned by using the contrasting tool in the software. A binary tool in the software separates the area covered by the bubbles and that of the water which is used in calculating the gas holdups for a particular matrix.

Actual gas velocities of the bubbles in each matrix were determined from the image processing tools for the void fraction calculation. Velocity is directly proportional to the distance travelled by a specific bubble and inversely related to the time it took the bubble to travel the distance. For the bubble regime, spherical bubbles were identified, within the transition regime, bubble caps were located and for the slug regime, Taylor bubbles were located and the distance travelled as the bubbles moved from the bottom or within the frame considered was recorded. The videos were taken in 240 frames per second mode; hence, specific bubbles could be identified as the flow progressed. The time taken for the bubbles to leave the frame was also recorded, and the velocities were computed from the velocity relation. Multiple velocities were calculated from the same video for a particular matrix and the final velocity used was the arithmetic average of the velocities.

Visual observation, a direct technique, was used in identifying the flow regimes for each matrix run. The shape, size, speed and distribution of the bubbles were used in differentiating the flow regimes. Flow regimes in a vertical column include bubbly, slug, churn, and annular flow. Bubbly, slug flow, and transition regimes were observed in the 3-in diameter given a maximum fluid flow rate of 16 l/min. The bubbly flow is characterised by numerous small bubbles that are uniformly dispersed throughout the liquid column. These bubbles move independently and do not significantly affect the overall flow pattern. The liquid surface appears relatively calm with no clear pattern of slugs or distinct gas pockets.

During the transition stage, as the gas flow rate or liquid velocity gradually increases, the behaviour of the bubbles changes. Initially, some bubbles start to coalesce, forming larger gas pockets. These larger pockets of gas intermittently push through the liquid column, causing minor fluctuations in the liquid. Once the transition is completed, the slug flow regime is established. To observe this transition, the gradual merging of bubbles into larger bubble caps leads to the formation of Taylor bubbles, that is, large bullet-shaped bubbles. The slugs will become more defined and evident as the transition progresses, eventually fully establishing the slug flow regime.

The coalesced bubble caps become more pronounced as the gas flow rate or liquid velocity continues to rise. The larger gas caps now clearly separate portions of liquid, resulting in the formation of distinct slugs of gas. These slugs alternate periodically as they move up the column. The liquid-gas interaction becomes visible and more turbulent due to the rapid movement of slugs and gas bubbles.

Results and Discussion

Measuring void fraction in two-phase flow involves converting flow videos into image frames and analysing pixel intensity to differentiate between liquid and gas phases. A camera captures 20-second videos of experimental runs, yielding 240 frames per second for analysis. However, factors like transparency, refractive index, and light angle affect pixel intensity, complicating void fraction determination from a single frame.

This is where employing an increased number of frames proves invaluable. Through averaging pixel intensities across numerous frames, the noise and uncertainty inherent in measurements can be mitigated by using the image processor-Image J software. This averaging process facilitates the compensation of effects caused by various factors over time, enhancing accuracy.

In general, augmenting the number of frames utilized directly corresponds to heightened accuracy in void fraction measurement. Nevertheless, a trade-off arises between accuracy and computational time. The more frames incorporated, the more computationally demanding the analysis becomes in terms of time. A pragmatic guideline recommends employing a minimum of 100 frames to achieve a satisfactory equilibrium between accuracy and computational efficiency. However, circumstances may necessitate a higher frame count. Instances include turbulent flows or exceptionally low void fractions, where additional frames are crucial to capturing dynamic changes or subtle variations that could escape detection with fewer frames.

In this work, 5 frames were used to determine the void fractions and other parameters, such as the flow regime. This

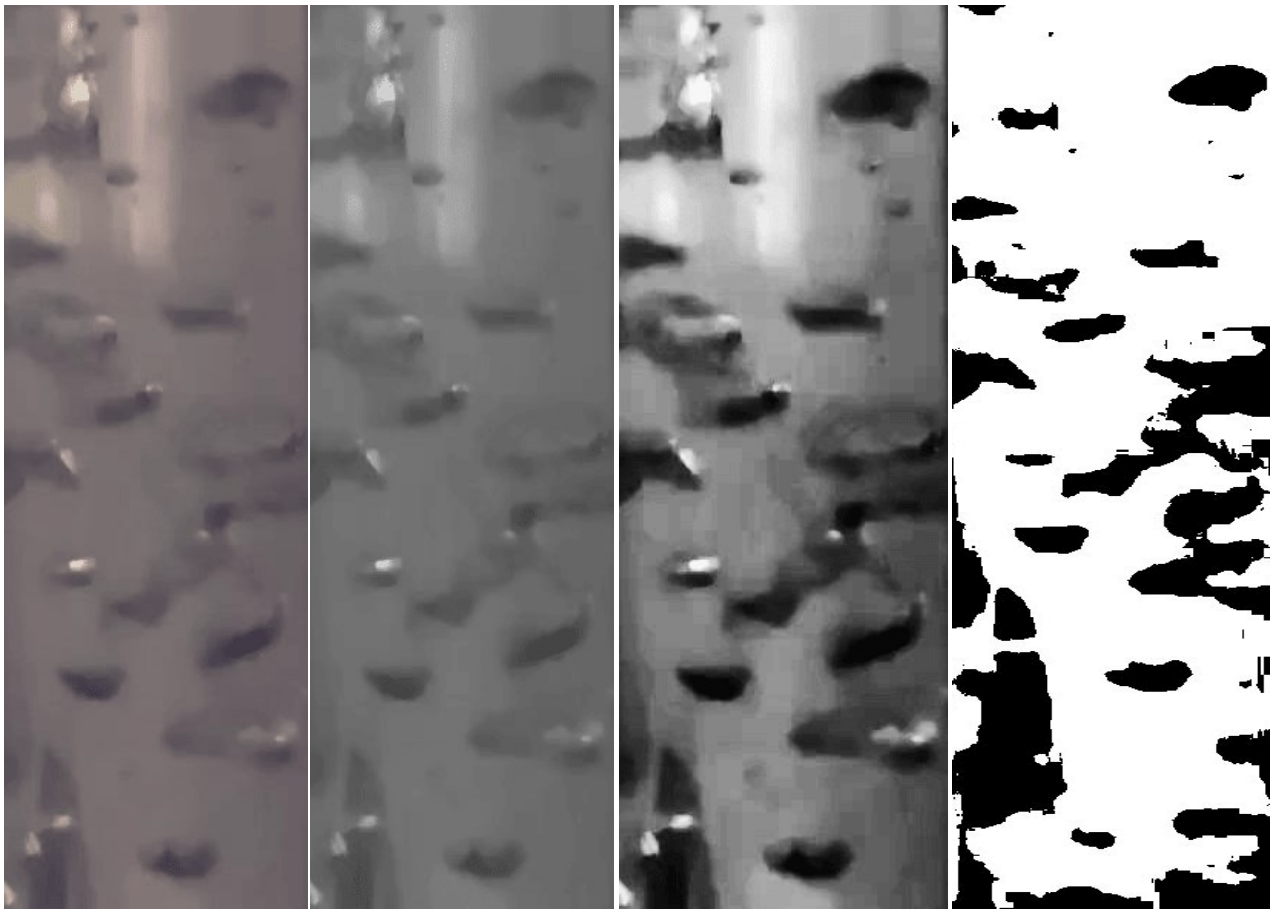

(a) RGB scale (b) Grayscale (c) Saturated (d) Binary scale

Figure 7 Stages of image processing for bubble identification: (a) RGB scale, (b) grayscale, (c) saturated, and (d) binary scale images

decision was made due to the proper consistency of the void fractions, as void fractions from using 1 frame up to 5 frames were considered. To further support this choice, Figure 8 illustrates the stability of gas holdup values beyond the fifth frame, where minimal variation is observed from frames 5 through 10. This stability indicates that increasing the number of frames beyond five does not significantly improve the accuracy of the gas holdup measurements. Instead, it only increases computational time without yielding further benefits. Therefore, selecting five frames strikes an optimal balance between computational efficiency and measurement accuracy.

As illustrated in Figure 8, gas holdup values remain stable even when using up to 10 frames, confirming that increasing beyond five frames does not significantly enhance measurement accuracy. Figure 9 presents the experimental void fractions derived from averaging five frames, supporting that this selected frame count provides consistent and reliable data for analysis within the study's context. Fluid dynamics in a bubble column reactor cannot be effective without understanding how the gas holdup correlates with other parameters in the research. Gas holdups are measured for a varying gas flow rate whilst maintaining the liquid flow rate. Generally, gas holds up increases with the superficial velocity of the gas which is computed from the gas flow rate. Experimental void fractions (ε_exp) or gas hold-ups are plotted together with predicted void fractions against the superficial velocity of the gas to know how each gas holdup behaves with an increasing gas superficial velocity and a constant liquid superficial velocity. The graphs are shown in Figure 10.

Initially, at low superficial velocities, the gas holdup remains relatively low due to insufficient gas momentum to overcome liquid inertia and establish efficient bubble dispersion. In this regime, smaller ellipsoidal bubbles are formed, leading to decreased interfacial area of the gas and limited gas-liquid interaction with the liquid. This can be seen in Figure 10. It can be observed from the Vsl = 0.00 m/s plot in Figure 10a that the homogenous and the Armand (1946) model gas holdups are constant at 1.00 and 0.83 respectively and this is because the homogenous model assumes uniform conditions and it depends on the ratio of the Vsg to Vm so when the Vsl is constant at 0.00m/s, the homogenous gas holdup will be constant for each of the Vsg at 1.0 for all the experimental matrices.

As the Vsg progressively rises, the larger bubbles ascend more rapidly through the liquid, further reducing their interaction time and limiting the gas holdup. The Armand (1946) model depends on the homogenous gas holdups by reducing the homogenous gas holdup by a factor, to cater for the slip between the gas and liquid. Hence, that also remains constant at 0.83. Also, it can be observed from Figures 10a to 10d that the experimental gas holdup increases until it gets to a point where there is non-linearity between the points. This is because as the Vsg continues to increase, a transitional region is encountered where the gas momentum becomes sufficient to overcome the liquid inertia, resulting in an improved bubble coalescence throughout the liquid.

It is important to note that the behaviour of gas holdup against Vsg is influenced by factors such as liquid properties (density, viscosity), gas properties (density, viscosity), column geometry (diameter, height), and column diameter. In a smaller -diameter column, for instance, the transition to efficient mixing occurs at lower gas superficial velocities due to reduced liquid inertia and shorter bubble residence times. Conversely, larger-diameter columns might require higher gas superficial velocities to initiate effective gas-liquid interaction.

Relationship between actual gas velocities and gas superficial velocities

Comparing gas superficial to the actual velocities shows that all Vsg values are smaller than the Vg. This is because the gas

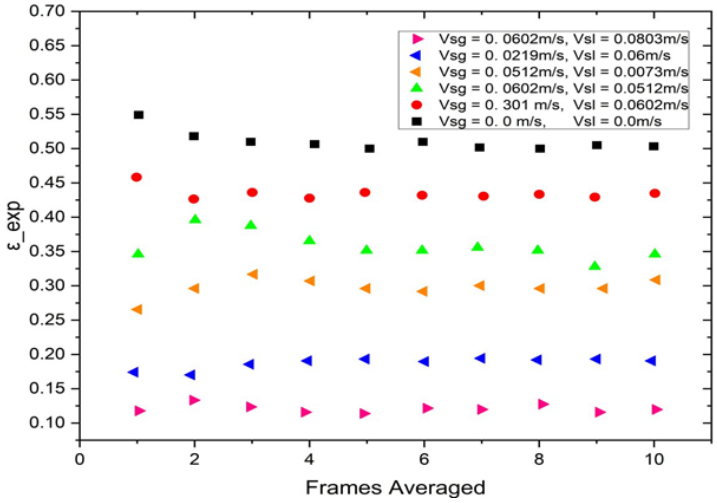

Figure 8 Stability of experimental gas holdup values across multiple frames, demonstrating consistency beyond five frames for different flow conditions

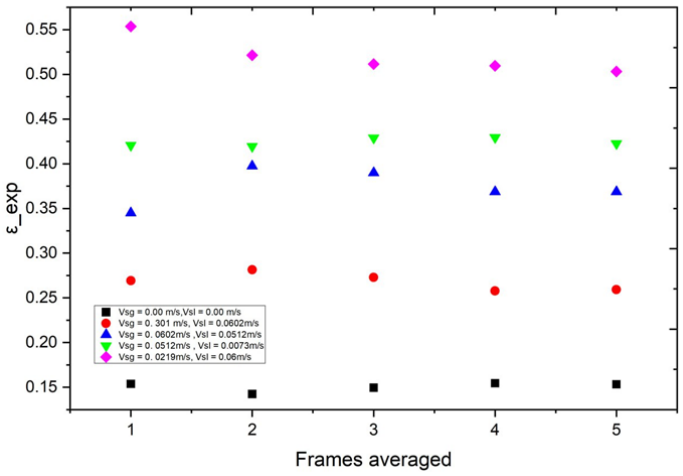

Figure 9 Experimental void fractions against the number of frames averaged

superficial velocities assume the whole cross-sectional area of the column while the actual gas velocities consider the area of the bubbles in the column. Analysing the trend between these two variables provides essential information about the bubble column's performance. The scatter plot created to represent this trend visually illustrates the relationship between actual gas velocities and superficial velocities. Each data point on the scatter plot in Figure 11a to 11d corresponds to a specific operational condition within the column at constant Vsl.

The trendline follows a linear pattern, which suggests a proportional correlation between actual gas velocities and superficial velocities. A positive slope indicates that as superficial velocities increase, the actual gas velocities increase, signifying an efficient transfer of gas through the liquid phase. The actual velocities increase with increasing gas superficial velocity because bubbles gain a higher momentum against the liquid fraction. For Taylor bubbles in the slug regime, the actual gas velocities are very high and erratic. These can be observed within the last six points of each of the plots in Figures 11a to 11d.

Factors such as bubble coalescence, breakup, and liquid viscosity could contribute to deviations from a linear relation. Moreover, the trend analysis might reveal an upper limit of actual gas velocities achievable under specific operating conditions. This could be due to limitations in bubble size and gas holdup.

In general, the trendline will be steeper for systems with higher fluid viscosities because the viscosity will create more resistance to the flow of the fluid, which requires a higher actual gas velocity to achieve a given superficial gas velocity. Understanding the trend between actual gas velocities and superficial velocities has practical implications for the design

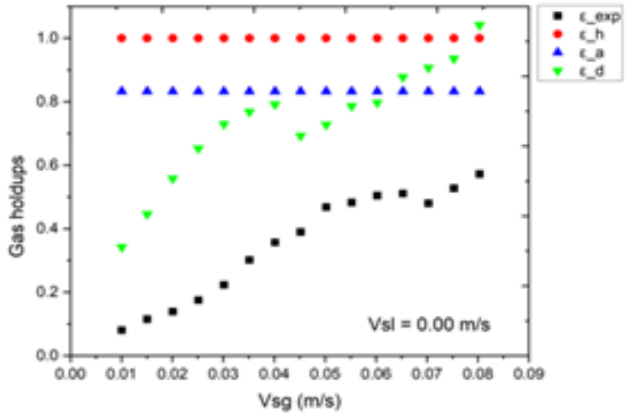

(a) vsl = 0.00m/s

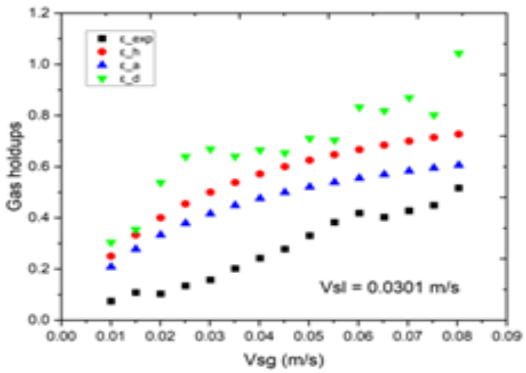

(b) vsl = 0.0301 m/s

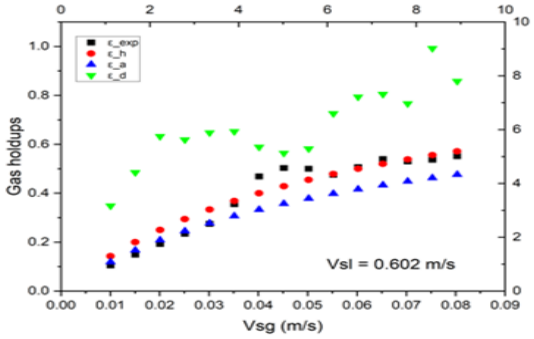

(c) vsl = 0.0602 m/s

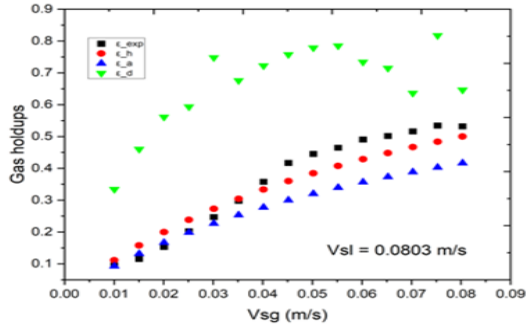

(d) vsl =0.0803 m/s

Figure 10 Gas holdup for constant superficial liquid velocity (Vsl) against varying superficial gas velocity (Vsg) for different models: (a) Vsl = 0.00 m/s, (b) Vsl = 0.0301 m/s, (c) Vsl = 0.0602 m/s, (d) Vsl = 0.0803 m/s

and optimization of bubble column processes. Engineers and researchers can utilise this analysis to determine the appropriate operational conditions that maximize gas-liquid interaction while avoiding inefficiencies such as flooding or channelling. Moreover, the trend analysis aids in identifying critical transition points where the bubble column behaviour might shift from one regime to another, impacting process efficiency.

The trend analysis of actual gas velocities against superficial velocities in a bubble column offers a comprehensive understanding of the gas-liquid interaction dynamics. Through scatter plots and trend lines, this analysis highlights the relationship between these two variables and uncovers crucial insights into the behaviour of gases within the column. This knowledge serves as a valuable tool for engineers and researchers engaged in designing, optimizing, and understanding bubble column processes, contributing to advancements in chemical engineering and process industries.

The superficial mixture velocity is a hypothetical velocity that is calculated as if the air and water phases were occupying the entire cross-sectional area of the flow channel. This is done to estimate the mixture velocity, even though the gas phase actually occupies a smaller fraction of the area. The actual gas velocity is the actual velocity of the air bubbles as it travels with the water. It is experimentally determined by finding the distance and time travelled by a group of bubbles for each matrix. The gas phase only occupies a fraction of the cross-sectional area, so its actual velocity is always higher than the superficial velocity of the liquid. The liquid flow rate is kept constant at intervals of 0.0100 m/s from 0.00 m/s to 0.0803 m/s, hence, nine different trends are recorded on the Vg against Vm (Vsl + Vsg) graph in Figure 12

Figure 12 illustrates the relationship between the actual gas velocity (Vg) and the mixture velocity (Vm). The drift velocity is determined at the point when the mixture velocity (Vm) is zero, which occurs when both the superficial gas velocity (Vsg) and the superficial liquid velocity (Vsl) are zero, indicating that there is no net flow of either gas or liquid in the system. At this point, the mixture velocity is also zero, and the drift velocity represents the relative motion of bubbles in a stagnant liquid.

A positive linear plot characterizes the general trend for the relationship between actual gas velocity and superficial mixture velocity. When Vsl = 0.00 m/s, Figure 12 shows that the actual velocity begins to deviate from the initial constant gradient, a trend that is also observed when Vsl is kept constant at 0.0201 m/s, with the initial points remaining linear until the mixture velocity exceeds 0.0600 m/s. At a constant Vsl of 0.0703 m/s, the graph remains linear with a nearly constant gradient until the mixture velocity reaches 0.12 m/s, after which the points scatter, indicating the transition from bubble to slug flow.

As gas introduction intensifies, bubble concentration increases leading to transitioning to a turbulent flow. In bubble column reactors, this transition is characterized by more significant bubble interactions, coalescence, and potential formation of froth at the liquid surface. Smaller bubbles enlarge as the gas's superficial velocity increases, which forms bubble caps and Taylor bubbles. This indicates the slug regime is reached.

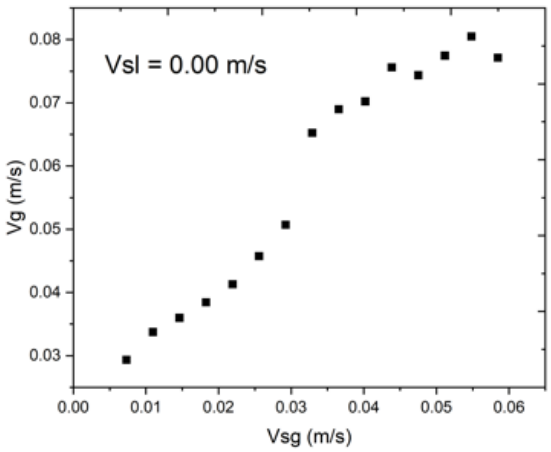

(a) vsl = 0.00m/s

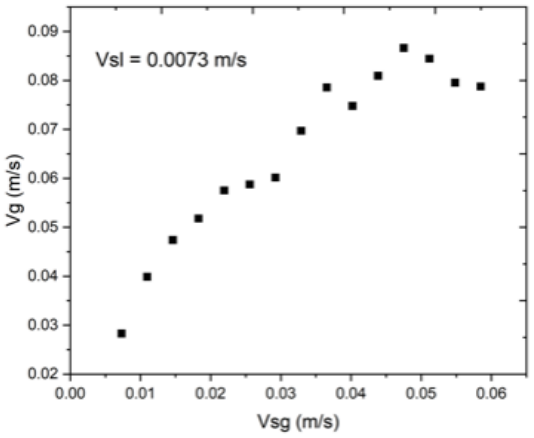

(b) vsl = 0.0073 m/s

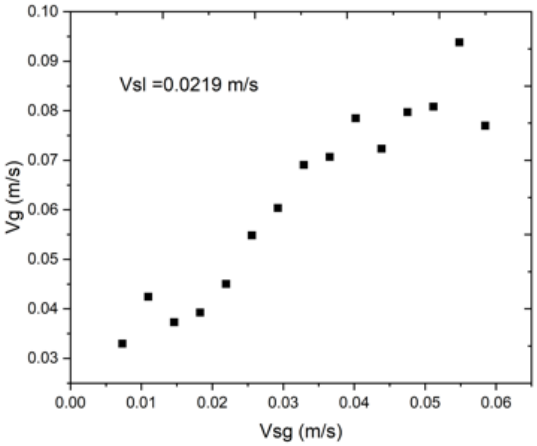

(c) vsl = 0.0219 m/s

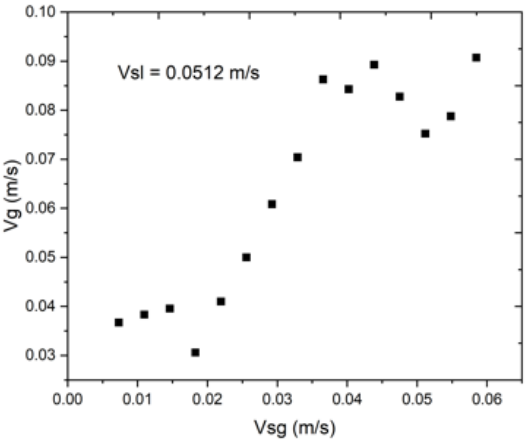

(d) vsl =0.0512 m/s

Figure 11 Velocity comparison for constant superficial liquid velocity (Vsl) against varying superficial gas velocity (Vsg) for different conditions: (a) Vsl = 0.00 m/s, (b) Vsl = 0.0073 m/s, (c) Vsl = 0.0219 m/s, (d) Vsl = 0.0512 m/s

As a result, the relationship between actual gas velocity and superficial mixture velocity becomes non-linear. It depends on several factors such as bubble size distribution, liquid viscosity, and reactor geometry. The comparison between the actual gas velocity and the mixture velocity is linked to an intriguing correlation called the Drift flux correlation. The drift flux correlation can be used in validating the gas holdup and other parameters. The correlation is given as:

$$V_g = C_o \,.\, (V_{sl} + V_{sg}) + V_{dg} \quad (12)$$

Where V_g is the actual gas velocity, C_o is the distribution coefficient, V_{sl} is the superficial liquid velocity, V_{sg} is the superficial gas velocity and V_{dg} is the gas drift velocity

Comparing Equation (12) to a regular linear equation, the distribution coefficient, C_o is the gradient when V_g is drawn against the mixture velocity. Zubar and Findlay (1965) stipulated that the C_o is constant at 1.19 for bubble flow and 1.20 for slug flow. The gas drift velocity, V_{dg}, therefore, represents the intercept on the V_g axis when the mixture velocity is extrapolated to zero. The drift velocity represents the difference between the rise velocity of bubbles through the liquid and the liquid's vertical flow velocity. The drift flux captures the relative movement between the gas and liquid phases, offering insights into the interaction and behaviour of bubbles within the reactor. It defines the terminal velocity of the gas when it is not accelerating or when the mixture velocity is zero. At that point, the bubbles move with a minimum velocity.

$$V_{dg} = 0.35\sqrt{gD} \quad (13)$$

The Equation (13) gives a gas drift velocity of 0.28 m/s which overestimates the experimental gas drift velocity approximately ten times. The gas drift velocity estimated from the experimental data is identified on the Vg against Vm. The gas drift velocity estimated from the plot in Figure 12 is 0.027 m/s and at that point, the actual gas velocities start increasing. The inconsistency between the experimental drift velocity and Taitel et al.'s 1980 model predictions suggests underlying factors such as variations in bubble size distribution, fluid properties, and phase interactions. Furthermore, unaccounted bubble interactions like coalescence and scaling discrepancies could also play significant roles. Resolving this difference is vital not only for aligning experimental observations with theoretical predictions but also for advancing the understanding of multiphase flow dynamics and improving the accuracy of predictive models in practical applications.

Parity plots

Parity plots are graphical representations used to compare two sets of data or models. Its main purpose is to assess the agreement and similarity between two data sets, in this case, the experimental and predicted gas holdups. This is achieved by plotting the predicted gas holdups against the experimental gas holdups to determine if the models suggested have been overestimated or underestimated.

Figure 13 shows a parity plot from data sets obtained when the superficial liquid velocity Vsl is kept constant at 0.0073 m/s. This plot compares the predicted gas holdups against experimental values, with deviations ranging from ±20% to ±50%, allowing assessment of model accuracy in predicting gas holdup under these conditions.

The 45-degree line in Figure 13 represents the ideal relationship between the data points plotted, where the predicted values are equal to the experimental values, hence any data point on the line represents no overestimation or underestimation. By analysing the distribution around the line of reference, the magnitude of deflection of the predicted gas holdups from the experimental gas holdups is estimated. From Figure 13, all the predicted gas holdup models deflect positively from the reference line due to overestimation with the homogenous model deflecting around 50% more than the experimental. The Armand model overestimates around 40% while the drift flux over-estimates the least around 20% and this analysis is valid when the Vsl is kept constant at 0.0073 m/s. Keeping the Vsl constant at 0.0292 m/s, the predicted gas holdups still overestimate the experimental gas holdup with a decreased margin of deflection. As shown in Figure 14, the margin of overestimation for the homogenous model is 26% which is almost the same as the Drift model which

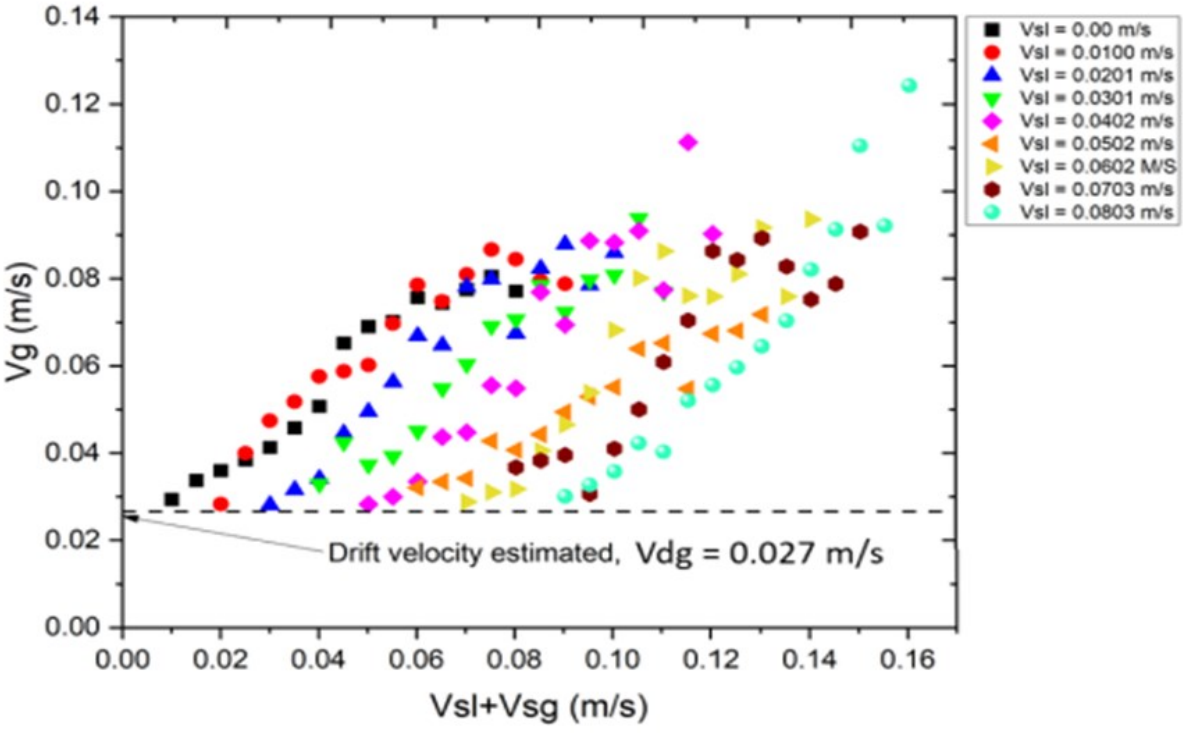

Figure 12 Relationship between actual gas velocity (Vg) and superficial mixture velocity (Vsl + Vsg), with drift velocity estimated at Vdg = 0.024 m/s for various Vsl values

overestimates the gas holdups by 25%. The Armand model margin of overestimation is reduced to 14% when the Vsl is kept constant at 0.0292 m/s.

Increasing the Vsl to 0.0512 m/s results in another parity plot with an interesting observation and this can be seen in Figure 15. The plot shows that the margin of deflection of the drift model's gas holdups still deflects positively from the experimental, by a a margin of 20%. The homogenous model however estimates the gas holdups slightly from the reference line with a margin of just 5%, with a few of the data points on the reference line. These experimental gas holdups are accurately predicted by the homogenous model.

Considering the Armands model in Figure 15, there is an underestimation of a margin of about 10% from the experimental gas holdups. This is reasonable and true since the Armands model is designed to always reduce the homogenous gas holds to cater for slip, other drag, and resistance not considered in the homogenous model. It can be inferred from Figure 13-14 that, as the Vsl increases, the accuracy of the models predicting the experimental gas holdup increases since after every increase in the Vsl, the margin of estimation from the reference line decreases.

Flow regime transition

The transition from bubble flow to slug flow occurs due to the agglomeration and coalescence of bubbles in the bubble flow regime at low liquid flow rates. Figure 16 visually depicts the observed flow regimes versus the predicted flow regimes during these transitions. The data points illustrate the gradual shift from dispersed bubble flow to slug flow, highlighting the complexities involved in predicting flow transitions. The comparison between observed and predicted flow regimes is essential for validating the models used in this study. Only in this way can the discrete bubbles combine into the larger vapor spaces, having a diameter nearly that of the tube, which is observed at the transition phase. As the gas rate is increased, the bubble density increases. This closer bubble spacing results in an increase in the coalescence rate. However, as the liquid rate increases, the turbulent fluctuations associated with the flow can cause the breakup of larger bubbles formed as a result of agglomeration. If this breakup is sufficiently intense to prevent coalescence, the dispersed bubble pattern can be maintained. Thus, to predict conditions for this transition, we must determine when each of these factors will dominate the process.

When gas is introduced at low flow rates into a large diameter vertical column of liquid (flowing at low velocity), the gas phase is distributed into discrete bubbles. Many studies of bubble motion demonstrated that if the bubbles are very small, they behave as rigid spheres rising vertically in rectilinear motion. However, above a critical size (about 0.15cm for air-water at low pressure) the bubbles begin to deform, and the upward motion is a zig-zag path with considerable randomness. The bubbles randomly collide and coalesce, forming several larger individual bubbles with a spherical cap similar to the Taylor bubbles of slug flow, but with diameters smaller than the pipe. Thus, even at low gas and liquid flow rates, bubble flow is characterized by an array of smaller bubbles moving in a zig-zag motion and the occasional appearance of larger, bubble caps.

The Taylor bubbles are not large enough to occupy the cross -section of the pipe to cause slug flow in the manner described above. Instead, they behave as free rising spherically capped voids, in the manner originally described by Sir Geoffrey Ingram Taylor. With an increase in gas flow rate, at these low liquid rates, the bubble density increases, and a point is reached where dispersed bubbles become so closely packed that many collisions occur and the rate of agglomeration to larger bubbles increases sharply. This results in a transition to slug flow. Experiments suggest that the bubble void fraction at which this happens is around 0.25 to 0.30. A semi-theoretical approach to

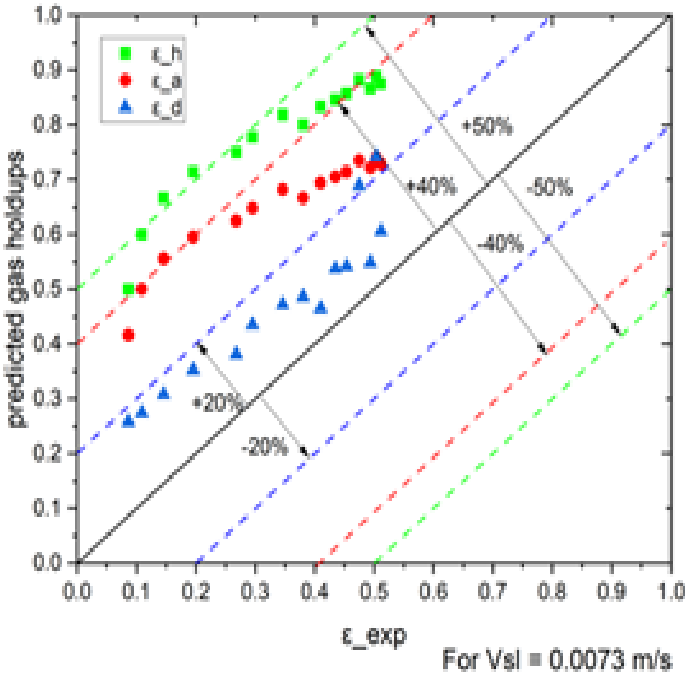

Figure 13 Parity plot of predicted gas holdups versus experimental gas holdups for Vsl = 0.0073 m/s showing deviations of ±20% to ±50%

this problem was given by Radovicich, et al., by considering a cubic lattice in which the individual bubble fluctuates. They postulated that the maximum void fraction is reached when the frequency of collision is very high, and it was shown that this happens around a void fraction of 0.30.

The observed slug flow data points in Figure 16 were in the bubble flow regime due to the nature of two-phase flow transitions. In fluid dynamics, the transition from one flow regime to another is not always clear-cut, and there can be overlaps. In the case of bubble and slug flows, the transition is a gradual process. As the gas flow rate increases, the bubbles in he bubble flow regime start to coalesce and form larger bubbles or 'slugs', leading to slug flow. However, this does not happen instantaneously at a certain point. There is a transition region where you can observe characteristics of both bubble and slug flows. This is why some slug flow data points are in the bubble flow regime. Moreover, specific conditions such as pressure, temperature, pipe diameter, and fluid properties can also influence these transitions. Therefore, depending on these factors, slug flow might be observed even under conditions typically associated with bubble flow. It is also worth noting that these are observed data points, which means they were

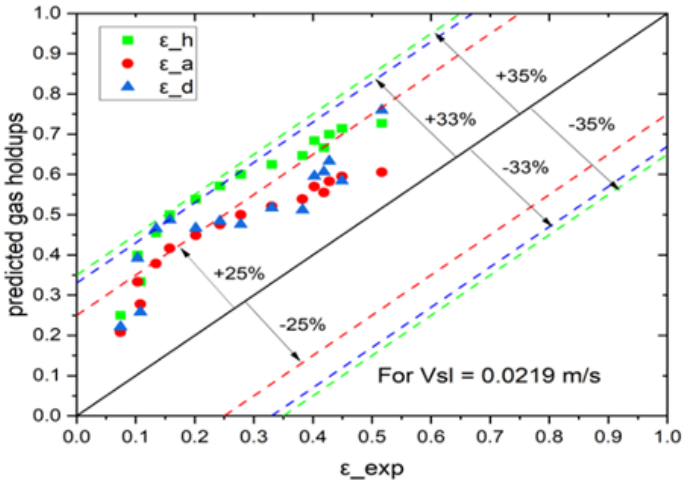

Figure 14 Parity plot of predicted gas holdups versus experimental gas holdups for Vsl = 0.0219 m/s showing deviations of ±25% to ±35%

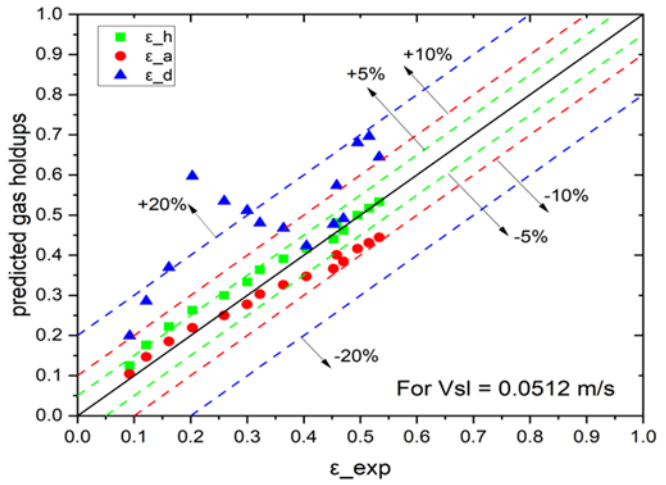

Figure 15 Parity plot of predicted gas holdups versus experimental gas holdups for Vsl = 0.0512 m/s, showing deviations of ±5% to ±20%

based on actual experiments. Experimental data can show some variability due to measurement uncertainty.

Conclusion

The investigation into flow regime transitions within bubble column reactors has unveiled the complexities and challenges associated with employing empirical models for prediction. While the homogenenous model effectively predicts bubble flow regimes, it shows limitations when applied to slug flow regimes, likely due to the complex interactions within the transitional regions. This phenomenon can be attributed to the inherent limitations of empirical models, which rely on simplified correlations and might struggle to capture intricate interactions and conditions within transitional regions. Factors such as sensitivity to parameters, overlapping regimes, and complex phase interactions contribute to the challenge of

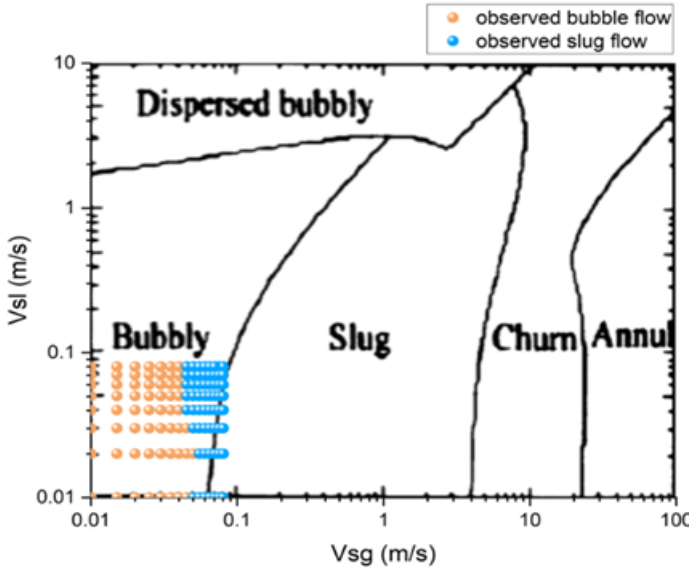

Figure 16 Observed flow regime (bubble and slug) against predicted flow regime map for various Vsl and Vsg values

predicting flow transitions accurately. These limitations highlight the necessity of integrating empirical models with advanced computational techniques, such as computational fluid dynamics (CFD), to improve predictive accuracy.

Refining and improving existing empirical models by incorporating more comprehensive data and insights into flow dynamics is essential. Validating models across a wide range of experimental conditions can elucidate their reliability in different scenarios and identify areas for improvement. Additionally, investigating transitional regions more closely and developing strategies to accurately predict behaviour within them is crucial. Furthermore, it is vital to account for experimental uncertainties and measurement errors when comparing model predictions with experimental data, as these factors can contribute to deviations between observed and predicted results.

Conflict of Interest Declarations

The authors declare no competing interests.

References

Armand, A.A. (1946). Counter current gas-liquid vertical flow, model for flow pattern and pressure drop. International Journal of Multiphase Flow, Volume 9, Issue 6, pp 637-647 https://doi.org/10.1016/0301-9322(83)90113-1

Armand, A.A. (1946). The resistance during the movement of a two-phase system in horizontal pipes. Izvestia Vses. Teplotekh. Inst., 1, 16-23.

B. Wu, M. Firouzi, T. Mitchell, T. E. Rufford C. Leonardi, B. Towler (2017). A critical review of flow maps for gas-liquid flows in vertical pipes and annuli. Chemical Engineering Journal, 326, pp. 350-377. https://doi.org/10.1016/j.cej.2017.05.135

Besagni, G., Brazzale, P., Fiocca, A., Inzoli, F. (2016). Estimation of bubble size distributions and shapes in two-phase bubble column using image analysis and optical probes. Flow Measurement and Instrumentation 52, pp. 190–207 https://doi.org/10.1016/j.flowmeasinst.2016.10.008

Cheng, L., Ribatski, G., Thome, J.R. (2008). Two-phase flow patterns and flow-pattern maps: fundamentals and applications. ASME. Applied Mechanics Review, 61(5): 050802. https://doi.org/10.1115/1.2955990

Dhaouadi, H., Poncin, S., Hornut, J., Midoux N. (2008). Gas–liquid mass transfer in bubble column reactor: Analytical solution and experimental confirmation. Chemical Engineering and Processing: Process Intensification, 47(4), pp. 548–556. https://doi.org/10.1016/j.cep.2006.11.009

Firouzi, M. and Hashemabadi, S. (2009). Analytical solution for Newtonian laminar flow through the concave and convex ducts (2009). ASME. Journal of Fluids Engineering.; 131(9): 094501 https://doi.org/10.1115/1.3184026

Gong, C.-K., Xu, X., Yang, Q. (2022). Gas holdup at dynamic equilibrium region of a bubble column: Effect of bubble generator performance. Chemical Engineering Journal, 443, 136382. https://doi.org/10.1016/j.cej.2022.136382

Hernandez-Alvarado, F., Kleinbart, S., Kalaga, D.V., Banerjee, S., Joshi, J.B., Kawaji, M. (2018). Comparison of void fraction measurements using different techniques in two-phase flow bubble column reactors. International Journal of Multiphase Flow, 102, pp. 119–129 https://doi.org/10.1016/j.ijmultiphaseflow.2018.02.002

Kaichiro, M., Ishii, M. (1984). Flow regime transition criteria for upward two-phase flow in vertical tubes. International Journal of Heat and Mass Transfer, 27(5), pp. 723–737 https://doi.org/10.1016/0017-9310(84)90142-X

Kantarci, N., Borak, F., Ulgen, K.O. (2005). Bubble column reactors. Process Biochemistry, 40(7), pp. 2263–2283 https://doi.org/10.1016/j.procbio.2004.10.004

Medjiade, W.T., Alvaro, A.R., Schumpe, A. (2017). Flow regime transitions in a bubble column. Chemical Engineering Science, 170, pp. 263–269 https://doi.org/10.1016/j.ces.2017.04.010

Mudde, R., Harteveld, W., Akker, H. (2009). Uniform flow in bubble columns. Industrial & Engineering Chemistry Research, 48(1), pp. 148–158 https://doi.org/10.1021/IE8000748

Nguyen, L.X., Ngo, S.I., Lim, Y.-I., Go, K.-S., Nho, N.-S.

(2022). Hydrodynamics of gas- liquid bubble columns under bubbling, transient, and jetting flow regimes using volume of fluid computational fluid dynamics. Chemical Engineering Research and Design, 182, pp. 616–628. https://doi.org/10.1016/j.cherd.2022.04.033

Nicklin, D. (1962). Two-phase flow in vertical tube. Chemical Engineering Science. 40, pp. 61–68. https://doi.org/10.1016/0009-2509(62)85027-1.

Radovcich, N.A. (1962). The transition from two-phase bubble flow to slug flow. PhD thesis, Massachusetts Institute of Technology

Shah, Y., Kelkar, B.G., Godbole, S., Deckwer, W.-D. (1982). Design parameters estimations for bubble column reactors. AICHE Journal, 28(3), pp. 353–379. https://doi.org/10.1002/aic.690280302

Shu, S., Vidal, D., Bertrand, F., Chaouki, J. (2019). Multiscale multiphase phenomena in bubble column reactors: A review. Renewable Energy, 141, pp. 613–631 https://doi.org/10.1016/j.renene.2019.04.020

Taitel, Y., Barnea, D., Dukler, A. (1980). Modelling flow pattern transitions for steady upward gas-liquid flow in vertical tubes. AIChE Journal 26(3), pp. 345–354 https://doi.org/10.1002/aic.690260304

Yamaguchi, K. and Yamazaki, Y. (1982). Characteristics of counter current gas-liquid two- phase flow in vertical tubes. Journal of Nuclear Science and Technology, 19(12), pp. 985–996. https://doi.org/10.1080/18811248.1982.9734247

Zahradnik, J., Fialova, M., Ru, M., Drahos, J., Kastanek, F., Thomas, N., et al. (1997). Duality of the gas-liquid flow regimes in bubble column reactors. Chemical Engineering Science, 52(21-22), pp. 3811–3826 https://doi.org/10.1016/S0009-2509(97)00226-1.

Zubar, N., Findlay, J. (1965). Average volumetric concentration in two-phase flow system. ASME, Journal of Heat Transfer 87(4), 453- 468. https://doi.org/10.1115/1.3689137